NASA/TM—1999-208501

Prediction of Heat and Mass Transfer in a Rotating Ribbed Coolant Passage With a 180 Degree Turn

David L. Rigby
NYMA, Inc., Brook Park, Ohio

Prepared for the
43rd Gas Turbine and Aeroengine Congress
sponsored by the International Gas Turbine Institute of
the American Society of Mechanical Engineers
Stockholm, Sweden, June 2–5, 1998

National Aeronautics and
Space Administration

Lewis Research Center

January 1999

Acknowledgments

The present work was supported by the NASA Lewis Research Center as part of the Coolant Flow Management Program with funding from the Smart Green Engine Project. The author wishes to thank Mr. Steven Hippensteele, Dr. Raymond Gaugler, Chief of the Turbine Branch, Mr. Ned Hannum, Chief of the Turbomachinery and Propulsion Systems Division as well as to Dr. Louis Povinelli, Chief Scientist of the Turbomachinery and Propulsion Systems Division of NASA Lewis Research Center, for their support and encouragement of this work. In addition, the author would like to thank Dr. Ali Ameri, Dr. Erlendur Steinthorsson, and Mr. Robert Boyle for their many insightful conversations on these types of flows.

Available from

NASA Center for Aerospace Information
7121 Standard Drive
Hanover, MD 21076
Price Code: A03

National Technical Information Service
5287 Port Royal Road
Springfield, VA 22100
Price Code: A03

Prediction of Heat and Mass Transfer in a Rotating Ribbed Coolant Passage with a 180 Degree Turn

David L. Rigby
NYMA, INC.
Brook Park, Ohio 44142
email: rigby@lerc.nasa.gov

ABSTRACT

Numerical results are presented for flow in a rotating internal passage with a 180 degree turn and ribbed walls. Reynolds numbers ranging from 5200 to 7900, and Rotation numbers of 0.0 and 0.24 were considered. The straight sections of the channel have a square cross section, with square ribs spaced one hydraulic diameter (D) apart on two opposite sides. The ribs have a height of 0.1D and are not staggered from one side to the other. The full three dimensional Reynolds Averaged Navier-Stokes equations are solved combined with the Wilcox k-ω turbulence model. By solving an additional equation for mass transfer, it is possible to isolate the effect of buoyancy in the presence of rotation. That is, heat transfer induced buoyancy effects can be eliminated as in naphthalene sublimation experiments. Heat transfer, mass transfer and flow field results are presented with favorable agreement with available experimental data. It is shown that numerically predicting the reattachment between ribs is essential to achieving an accurate prediction of heat/mass transfer. For the low Reynolds numbers considered, the standard turbulence model did not produce reattachment between ribs. By modifying the wall boundary condition on ω, the turbulent specific dissipation rate, much better agreement with the flow structure and heat/mass transfer was achieved. It is beyond the scope of the present work to make a general recommendation on the ω wall boundary condition. However, the present results suggest that the ω boundary condition should take into account the proximity to abrupt changes in geometry.

NOMENCLATURE (All quantities are dimensionless)

A	flow area
C_f	friction coefficient, $2\tau_w/\rho V^2$
D	hydraulic diameter or turbulent dissipation
e	rib width
h	heat transfer coefficient
h_m	mass transfer coefficient
k	thermal conductivity or turbulent kinetic energy
K_R	equivalent sand grain roughness height
l	turbulent length scale, $\sqrt{k}/\omega$
$\dot{m}$	mass flow rate
Nu	Nusselt number, hD/k
P	pressure or production of k
Pr	Prandtl number
Re	Reynolds number, VD/ν
Ro	rotation number, $\Omega D/V$
Sc	Schmidt number
Sh	Sherwood number, $h_m D/\Lambda$
T	dimensionless Temperature
V	characteristic velocity, $\dot{m}/(\rho A)$
y^+	dimensionless distance from the wall, $\frac{\eta}{D} Re \sqrt{\frac{C_f}{2}}$
ε	turbulence dissipation rate
η	distance normal to wall
γ	specific heat ratio
Λ	diffusion coefficient
μ	viscosity
ρ	density
ν	kinematic viscosity
Ω	vorticity or Rotation rate of channel
ω	specific dissipation of turbulence, $\frac{\varepsilon}{k}$
τ_w	wall shear stress

Subscripts

b	mass averaged or bulk value
$cent$	centerline value
in	condition at inlet
t	total condition or turbulence quantity
w	wall value
0	fully developed value

INTRODUCTION

Future generations of ultra high bypass-ratio jet engines will require far higher pressure ratios and operating temperatures than those of current engines. For the foreseeable future, engine materials will not be able to withstand the high temperatures without some form of cooling. In particular the turbine blades, which are under high thermal as well as mechanical loads, must be cooled (Taylor, 1980, Suo, 1978 and Snyder and Roelke, 1990). Cooling of turbine blades is achieved by bleeding air from the compressor stage of the engine through complicated internal passages in the turbine blades (internal cooling, including jet-impingement cooling) and by bleeding small amounts of air into the boundary layer of the external flow through small discrete holes on the surface of the blade (film cooling and transpiration cooling). The cooling must be done using a minimum amount of air or any increases in efficiency gained through higher operating temperature will be lost due to added load on the compressor stage.

Turbine cooling schemes have traditionally been based on extensive empirical data bases, quasi-one-dimensional computational fluid dynamics (CFD) analysis, and trial and error. With improved capabilities of CFD, these traditional methods can be augmented by full three-dimensional simulations of the coolant flow to predict in detail the heat transfer and metal temperatures. Several aspects of turbine coolant flows make such application of CFD difficult, thus a highly effective CFD methodology must be used. First, high resolution of the flow field is required to attain the needed accuracy for heat transfer predictions, making highly efficient flow solvers essential for such computations. Second, the geometries of the flow passages are complicated but must be modeled accurately in order to capture all important details of the flow. This makes grid generation and grid quality important issues. Finally, since coolant flows are turbulent and separated the effects of turbulence must be modeled with a low Reynolds number turbulence model to accurately predict details of heat transfer.

The overall objective of our ongoing research is to develop a CFD methodology that can be used effectively to design and evaluate turbine cooling schemes. In this study, we focus on two aspects of CFD for turbine cooling, namely grid structures for coolant passage geometries and turbulence modeling for coolant flows. Grid generation for complicated geometries such as coolant passages, is currently an active area of research. In general, grid systems for complicated geometries are classified as block-structured, unstructured or hybrid. Of those, unstructured grids offer the greatest flexibility for modeling of complex geometries and the generation of unstructured grids is largely automatic. In contrast, fully continuous block-structured grids, where all grid lines are at least C^1 continuous across block faces (here referred to as multi-block grids), are more difficult to generate but are the most suitable for simulations of viscous flows. In addition, flow solvers for structured grids typically require less memory than those for unstructured grids, and can take full advantage of various convergence acceleration schemes (e.g. multigrid) and fast solvers for implicit discretizations (e.g., line Gauss-Seidel, approximate LU and ADI schemes). In this study, we use semi-automatically generated multiblock grids (i.e., shape of blocks is automatically determined but grid-topology or block-structure needs to be specified beforehand).

Turbulence models used in simulations of internal flows in complicated geometries must be able to model flows involving separation and adverse pressure gradients. One such model is the k-ω model of Wilcox(1994a and 1994b). This model has several desirable features. One important feature is that it does not require distance to a nearest wall as a parameter. Second, the low Reynolds number version of the model can be used to model transition (Wilcox, 1994b). Finally, as both k and ω are well behaved numerically, stiffness associated with low-Reynolds number k-ε turbulence models is eliminated. In addition recent work by Chima (1996) show the model to be useful for predicting heat transfer over turbine blades.

The present code, TRAF3D.MB, was used previously for flow and heat transfer in rectangular ducts with a 180 degree turn, Rigby et al. (1996a) and also for a straight channel with ribs and bleed holes, Rigby et al. (1997).

There is extensive literature available on the study of rib roughened surfaces. Some examples of experimental work include Boyle (1984), Chen et al. (1996), Hibbs et al. (1997), Rau et al. (1996), Shen et al. (1994), and Taslim et al. (1995). Some examples of numerical work is this area includes Stephens et al. (1995a, 1995b), Stephens et al. (1996), and Stephens and Shih (1997).

For rib roughened channels with rotation, the work of Park (1996), and Park et al. (1997) offer local mass transfer distributions. Regional measurements of heat transfer are available in Wagner et al. (1992).

Mass transfer is often used experimentally to infer the heat transfer coefficients. Mass transfer experiments are more easily conducted, especially for rotating cases. The drawback of using mass transfer to simulate heat transfer is that buoyancy effects which arise due to rotation are completely eliminated. In the present numerical work an additional equation for concentration has been added to more closely match the mass transfer experimental conditions. In the future, the additional equation will also allow the study of the effect of buoyancy.

The remainder of this paper is organized as follows: After this introduction, the test problem is described. Then the numerical method used in the simulations is outlined and boundary conditions used to obtain proper entrance flow conditions are described. Subsequently, the grid systems used for the simulations are discussed, and the k-ω turbulence model and its implementation is described. Finally, the results of the computations are shown and compared to the experimental data. A total of six cases are presented with Reynolds numbers ranging from 5200 to 7900 and rotation numbers of 0.0 or 0.24. Investigation of the flow structure is presented as well as

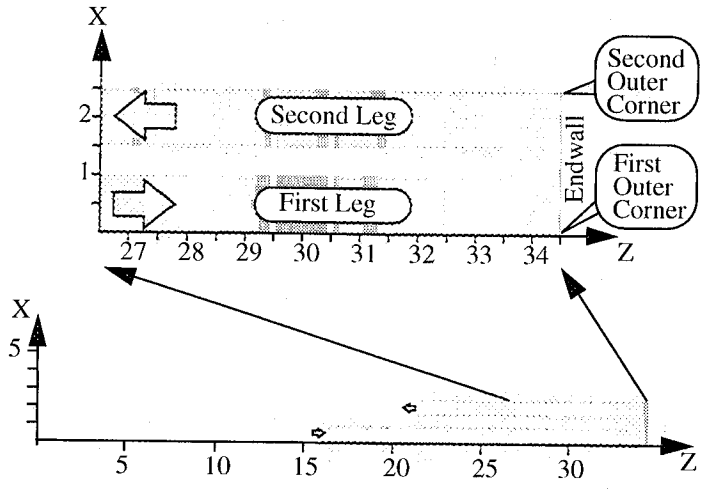

Fig. 1. Schematic of geometry

comparison of heat/mass transfer coefficients to experimental data. The paper ends with a summary and conclusions.

DESCRIPTION OF PROBLEM

The geometry, shown in Fig. 1, consists of two straight passages connected by a 180 degree turn. This geometry was chosen to match the experiments of Park (1996). The passages have a square cross section, and have ribs on two sides in the active section. All geometrical quantities are expressed relative to the hydraulic diameter. The active section consists of the turn region, and the upstream and downstream legs within seven hydraulic diameters of the turn. The inlet leg has an additional 10 hydraulic diameter long section which is smooth. The exit leg has an additional 5 hydraulic diameter long section which is also smooth. These smooth sections, as well as the ribs, do not allow any mass transfer or heat transfer in any of the calculations. The ribs are spaced one hydraulic diameter apart and have a height of one tenth of the hydraulic diameter.

Rotation is imposed about the x-axis. In the frame of reference rotating with the passage, the straight channels are aligned with the z-axis. The inlet to the first leg is at z=16.5, while the exit of the second leg is at z=21.5. The active section of the legs extend from z=26.5 to z=33.5. The turn region, which is also active, extends to z=34.5. The average radius of the active leg sections is 30 hydraulic diameters.

COMPUTATIONAL METHOD

Remarks on the code. The simulations performed in this study were done using a computer code called TRAF3D.MB (Steinthorsson et al. 1993). This code is a general purpose flow solver, designed for simulations of flows in complicated geometries. The code is based on the TRAF3D code, an efficient computer code designed for simulations of flows in turbine cascades (Arnone et al. 1991). The TRAF3D.MB code employs the full compressible Navier-Stokes equations. It uses a multi-stage Runge-Kutta scheme to march in pseudo time. The code utilizes multi-grid and implicit residual smoothing to accelerate convergence to steady state. Convective and diffusive fluxes are computed using central differencing. Artificial dissipation is added to prevent odd-even decoupling. The discretizations are formally second order accurate. To handle complex geometries, the code uses contiguous multiblock grid systems but has the added capability of handling grids with non-contiguous grid lines across branch cuts. For contiguous systems, all internal boundaries are conservative. The TRAF3D.MB code was described in detail by Steinthorsson et al. (1993). Some aspects of the formulation used in the code are the same as those described by Arnone et al. (1991). For the present computations the code was fitted with the low Reynolds number k-ω model of Wilcox (1994b).

An additional equation, a concentration equation was added to the code to allow for the calculation of mass transfer under adiabatic conditions. The purpose of adding this additional convection-diffusion equation was to simulate naphthalene sublimation experiments which do not experience the effects of buoyancy that a heated rotating channel would experience. The alternative would have been to attempt to impose a small temperature difference to minimize the effects of buoyancy. However, to obtain accurate heat transfer coefficients it is not advisable to impose extremely small temperature differences. The concentration equation, of course, depends on the solution of the other equations, but has no effect on them. A Schmidt number and turbulent Schmidt number of 2.28 and 0.9 were used respectively. Park (1996) has quoted a Schmidt number of 2.28 for Naphthalene sublimation. The Prandtl number and turbulent Prandtl number specified were 0.72 and 0.9, respectively.

With the addition of the concentration equation, it will be possible in future projects to isolate the effects of buoyancy and to study the combined effects of heat and mass transfer simultaneously.

Turbulence Model. When working with complicated geometries it is advantageous to use a set of equations describing the turbulence that does not require the computation of the dimensionless distance to the wall y^+. The boundaries between adjacent blocks should be free to cut across boundary layers and regions of high shear. Having to carry information on solid walls and dealing with corners requires communication of much information that is quite cumbersome and time consuming both in terms of programming and CPU time.

The k-ω turbulence model developed by Wilcox (1994a,1994b) satisfies our requirements. Modifications by Menter (1992,1993) improved the robustness of the model. Chima (1996) incorporated some of the latter modifications to the turbulence model and presented some applications of this model in the context of a Navier-Stokes solver. In fact it is the three-dimensional variation to the formulation adapted by Chima that has been utilized in this paper. Chima has shown the model to possess very good convergence properties. He also

showed that the model performs well in predicting the rate of heat transfer from a simulated flat plate and turbine blades under various conditions. Below we present the dimensionless equations describing the turbulence in tensor notation.

$$(\rho s_i)_{,t} + (\rho s_i u_j + q_{ij})_{,j} = (P_i - D_i) \tag{1}$$

$$q_{ij} = -Re^{-1}\left(\mu + \frac{\mu_t}{\sigma}\right)s_{i,j} \quad j=1,3 \tag{2}$$

where $s_1=k$ and $s_2=\omega$ also $\mu_t=\alpha^* \frac{\rho k}{\omega}$.

The source terms, P_i, of equation (1) are defined as

$$\boldsymbol{P} = \begin{bmatrix} Re^{-1} \cdot \mu_t 4\Omega^2 - \frac{2k\rho}{3}(\nabla \bullet V) \\ \rho\alpha\left[\alpha^* 4\Omega^2 - \frac{2}{3}\omega(\nabla \bullet V)\right] \end{bmatrix} \tag{3}$$

where Ω is the magnitude of the vorticity. The destruction terms, D_i, are given by

$$\boldsymbol{D} = \begin{bmatrix} \beta^*\rho\omega k \\ \beta\rho\omega^2 \end{bmatrix} \tag{4}$$

The coefficients appearing in the model are

$\sigma=2.0$, $\beta=3/40$, $\beta^*=0.09F_\beta$, $\alpha=(5/9)(F_\alpha/F_\mu)$, and $\alpha^*=F_\mu$, where

$$F_\beta = \frac{\frac{5}{18} + \frac{Re_T^4}{R_\beta}}{1 + \frac{Re_T^4}{R_\beta}}, F_\alpha = \frac{\alpha_0 + \frac{Re_T}{R_\omega}}{1 + \frac{Re_T}{R_\omega}}, F_\mu = \frac{\alpha_0^* + \frac{Re_T}{R_k}}{1 + \frac{Re_T}{R_k}} \tag{5}$$

Above $\alpha_0=0.1$, $\alpha_0^*=0.025$, $R_\beta=8$, $R_\omega=0.27$, $R_k=6$ and $Re_T = \rho k/\mu\omega$.

Boundary Conditions. The types of boundary conditions encountered in solving the problem at hand are as follows:

1) Inlet: The inlet boundary condition for subsonic flows is treated by specifying the relative total temperature and relative total pressure as well as the inlet angle profiles. The outgoing Riemann invariant is extrapolated to the inlet from within. The total temperature and total pressure profiles are chosen to produce specified velocity and temperature profiles. In the present work, a flat profile is assumed at the inlet. The flow is assumed to be aligned with the channel in the relative frame of reference. This was assumed because in the experiment, the test section is encased in a perforated containment tube. The inlet value of turbulence intensity was set to 4% and the length scale to 0.14D. Inlet values of k and ω are set based on μ_t and l. The inlet value of the concentration was set to zero.

2) Exit: At the exit boundary, for subsonic flow, the pressure is specified while all other conditions are extrapolated from within.

3) Walls: At walls, the normal pressure gradient is set to zero, either the temperature or heat flux is specified, and the no-slip condition is enforced. The density and total energy are computed from the pressure and the temperature. The boundary conditions for the turbulence quantities are $k=0$ and

$$\omega = S_R \frac{\partial u}{\partial y}\bigg|_{wall} \quad \text{where, } S_R = \begin{bmatrix} \left(\frac{50}{K_R}\right)^2, K_R < 25 \\ \frac{100}{K_R}, K_R \geq 25 \end{bmatrix} \tag{6}$$

and K_R is the equivalent sand grain roughness height in turbulent wall units. This condition on ω is attributable to Wilcox. A discussion on the physical reasoning behind the condition can be found in Wilcox (1988). Two values of K_R were examined. A value of 5 corresponding to a hydraulically smooth surface, and a value of 36 which is roughly the height of a rib in wall units (i.e. y^+).

An upper limit is imposed on the value of ω at the wall using the following boundary condition suggested by Menter(1993) and found effective by Chima(1996),

$$\omega_{max} = \frac{10}{Re} \cdot \frac{6}{\beta} \cdot \frac{\nu}{\Delta y^2} \tag{7}$$

On active walls, the dimensionless concentration was set to 1. For inactive walls the gradient of the concentration and heat flux was set to zero. For cases with imposed temperature differences, the wall temperature was set to $1.2T_{t,in}$ on all surfaces where the mass transfer was active. The active regions included all the walls of the corner region, as well as the four walls of each leg within seven hydraulic diameters of the corner. The ribs themselves were not active, and the inlet and exit sections were not active.

COMPUTATIONAL GRID

The structured multiblock grid used for the present work was generated using the commercially available package, GridPro (1993). With this package it is relatively easy, compared to other available packages, to generate a topology around one rib and then copy it to each rib in the geometry. Figure 2 shows the grid in the plane x=0. In Fig. 2 one can see how the grid is designed to follow the viscous boundaries. Having grid lines remain attached to the viscous boundaries improves computational efficiency, since viscous grids are not allowed to propagate into the inviscid region where they are not needed.

Figure 3 shows the grid at y=0. Notice that viscous grids are confined to the near wall regions. This figure also shows how high quality grids are obtained near the outer corners of the turn. By not allowing the grid to wrap around the outer corners, significant improvement in grid orthogonality is obtained.

The GridPro software generates all full face matching blocks. This has a tendency to produce many small blocks, which is in general detrimental to computational efficiency, so

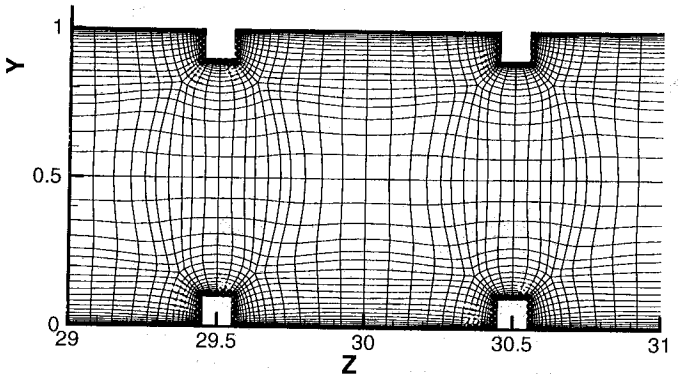

Fig. 2. Grid in the plane x=0

they are merged into a smaller number of blocks. The grid system just described was made up of 288 full face matching blocks. Before the computations are begun, the grid system was merged down to 64 blocks using the Method of Weakest Descent of Rigby (1996b) and Rigby et al. (1997). The method has been demonstrated to be very effective at merging multiblock grids to a minimum number of blocks. The block merging ability is now included as part of the GridPro package.

The procedure for grid generation is to first produce an inviscid grid, then the viscous grid is generated by embedding grid lines near solid surfaces. The first grid space from the wall is chosen so that the largest y^+ value of a cell center is approximately unity. The stretching ratio away from the wall is limited to less than 1.25. The grid contained 1,489,920 cells. This level of grid density has yielded good results in the past work with this code (Rigby et al. 1996a, 1997). Each case used approximately 30 to 40 hours of CPU time on a CRAY C90.

RESULTS AND DISCUSSIONS

Overview of Results. A total of six cases will be discussed. Table 1 shows a summary of the conditions. The first three cases are referred to as sta5, sta5heat, and rot5. Case sta5 is stationary and adiabatic, while case sta5heat is stationary with wall temperatures of $1.2T_{t,in}$. The case rot5 is an adiabatic rotating case with a rotation number of 0.233. Each of these cases, containing the number 5, use K_R=5. The next three cases

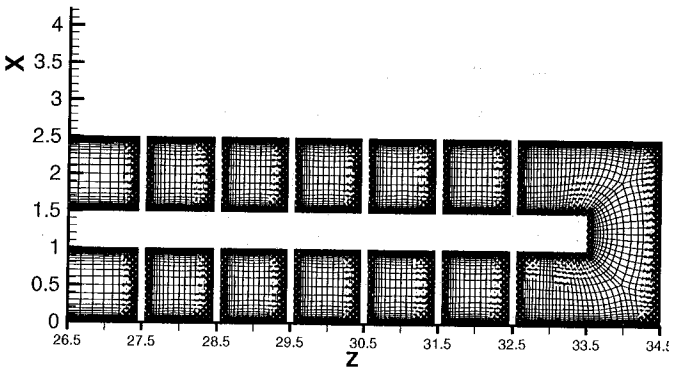

Fig. 3. Grid in the plane y=0.0

Case	$T_w/T_{t,in}$	Re	M_{in}	Ro	K_R
sta5	adiabatic	7712	0.1195	0.00	5
sta5heat	1.2	6971	0.1169	0.00	5
rot5	adiabatic	5481	0.1028	0.233	5
sta36	adiabatic	7872	0.1220	0.00	36
sta36heat	1.2	6722	0.1130	0.00	36
rot36	adiabatic	5250	0.0984	0.244	36

TABLE 1. Summary of cases.

sta36, sta36heat, and rot36 are the same as the first three except with K_R=36.

The computed cases with K_R=5 showed almost no signs of reattachment between the ribs, as shown in the velocity vector plots in the next section. In general for a ratio of pitch to rib height of 10, experiments show reattachment occurring around midway between the ribs. It is believed that the lack of reattachment may demonstrate a weakness in the turbulence model at these low Reynolds numbers. Previous calculations (Rigby et al. 1997) with this code, on a channel with ribs on one side, produced the expected reattachment with Reynolds numbers above 10,000. In modern engines the Reynolds number in the coolant passage is generally 25,000 to 100,000. The Rotation numbers in this study are comparable to engine conditions.

An ad hoc attempt was made to modify the boundary condition on ω at the wall to improve the predictions. A value of K_R of 36 was chosen for two reasons. First, to produce an improved solution K_R needed to be increased. Second, a value of 36 was chosen because it is roughly the height of the rib in wall units and is significantly smaller than the equivalent roughness height. An equivalent roughness height on the order of 10 times the rib height would be expected for this type of geometry (Sigal and Danberg, 1990).

The cases with K_R=36 showed a dramatic improvement compared to the previous runs. Reattachment was observed between the ribs and the heat/mass transfer values were significantly increased to levels in the range measured experimentally. Given the computational requirements of the present geometry, it is beyond the scope of the present work to fully test the effects of varying K_R. However, it is quite possible that the specific value chosen for K_R may not be as important as producing the reattachment. That is to say, if two values of K_R produce reattachment the flow field may be relatively insensitive to the exact value chosen. The relatively good agreement of the present results lends credence to the previous statement. However, this hypothesis will need to be tested more thoroughly on a simpler problem at a later date.

In the following sections, the aerodynamic effects are discussed, then the heat/mass transfer results are discussed.

The Flow Field and Pressure Distribution. There are two topologically interesting regions to discuss. The first is the flow between the ribs, and the second is the flow in the turn region.

Experimental observations for ribs with a pitch to height ratio of ten show the flow around the ribs is dominated by three or possibly four vortex structures. A fairly large separation zone should extend to about 4 rib heights downstream of the rib followed by a reattached region which separates once again about one rib height upstream of the next rib. The third vortex is a contra-rotating vortex just downstream of the rib. The possible fourth vortex structure exists on top of the rib, and is very small. This flow structure has been observed by several researchers. An example can be found in Rau et al. (1996). Figure 4a shows velocity vectors at x=0.5, the middle of the channel, between the fourth and fifth ribs for the case sta36. Note, only one fourth of the velocity vectors used in the calculation are shown in the figure. This figure demonstrates that the expected flow structure is produced for this case which has K_R=36. Figure 4b shows the same region for the case sta5 which has K_R=5. Notice that Fig. 4b shows separation spanning the entire distance between the ribs. Figures 5a and 5b show the same regions for the rotating cases rot36 and rot5, respectively. Similar improvement with regard to the reattachment is observed for the rotating cases. The propagation of fluid toward the trailing wall (y=1) is also visible in Fig 5.

Flow in the turn region at y=0.5, for the stationary case sta36 is shown in Fig 6a. The flow is seen to impinge on the endwall. As the flow turns, separation regions appear near the first outside corner as well as around the sharp inside corner. In addition a small separation zone is observed near the second outside corner. Figure 6b shows the flow in the turn region for the rotating case rot36. The flow is much like the stationary case, with the exception that the separation around the inside corner is greatly diminished.

By looking at a cross section at x=1.25 the strong secondary flow in the turn can be seen. Figure 7a shows the flow forming a strong double vortex, due to symmetry for the case sta36. Two additional weaker vortices are seen near the inside turn (z=33.5). Figure 7b shows the flow at x=1.25 for the rotating case rot36. Notice that the symmetry is lost due to the rotation. The flow in the plane x=1.25 for the rotating is dominated by one large vortex, with smaller vortices visible near the corners of the cross section.

Studying the pressure distribution in the channel can be helpful in demonstrating pressure loss and form drag on the ribs. The pressure will be presented in terms of a what will be termed a relative pressure coefficient defined by:

$$C_{p,rel} = \frac{p - p_{1D}}{\frac{\rho}{2} \cdot U_{in}^2} \qquad (8)$$

where p_{1D} is the pressure predicted by a one dimensional theory assuming inviscid radial flow in a rotating tube. (Stephens et al.

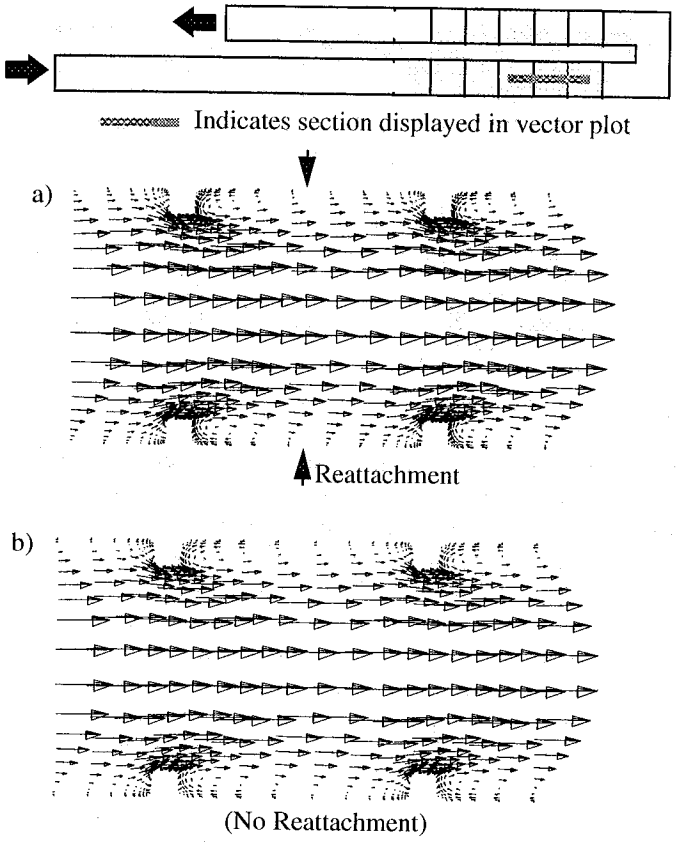

Fig. 4. Velocity vectors at x=0.5 in the range 30<z<32, a) case sta36, b) case sta5. (Coarsened by factor of two for plotting)

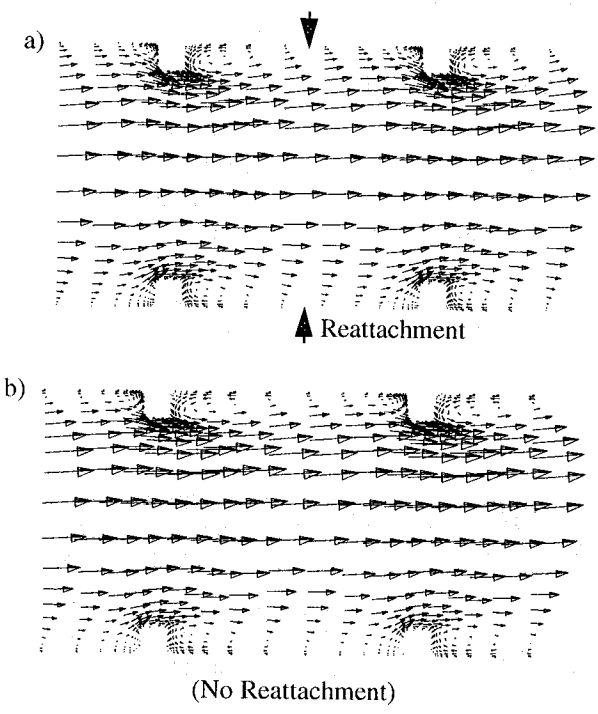

Fig. 5. Velocity vectors at x=0.5 in the range 30<z<32, a) case rot36, b) case rot5. (Coarsened by factor of two for plotting)

a) sta36 b) rot36

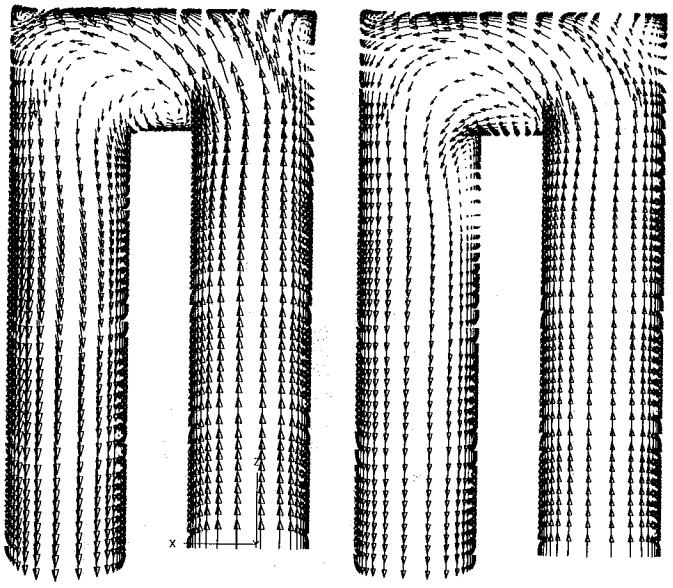

Fig. 6. Velocity vectors at y=0.5 in the range 30<z<34.5, a) case sta36, b) case rot36. (Coarsened by factor of two for plotting)

1996). From the theory presented in Stephens et al. (1996) it can be deduced that:

$$p_{1D} = p_{ref}\left(1 + \frac{\gamma - 1}{2} M_{in}^2 Ro^2 (z^2 - z_{in}^2)\right)^{\gamma/(\gamma-1)} \qquad (9)$$

where p_{ref} is the inlet static pressure.

It is interesting to note that for the present flow conditions a pressure increase of roughly 40% occurs between the inlet and the endwall. This increase is very accurately predicted by the one dimensional analysis. It is also interesting to note that the predicted pressure increase is independent of the flow rate. Notice the combination of $M_{in}Ro$ in equation 13. This combination can be thought of as a compressible rotation number. In actual engines this would have a value on the order of the value used in these calculations, that is 0.024. In most experiments this value would be much lower due to safety constraints on rotational speed.

a) sta36

b) rot36

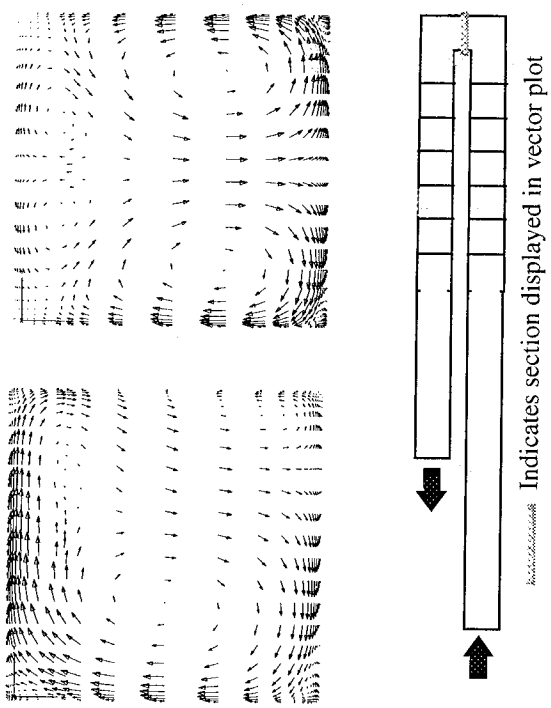

Fig. 7. Velocity vectors in the plane x=1.25, a) case sta36, b) rot36. (Coarsened by factor of two for plotting)

Figure 8a shows $C_{p,rel}$ for the case sta36. For this stationary case the values at y=0 and y=1 are identical due to symmetry. From Fig. 8a it can be seen that a gradual drop in $C_{p,rel}$ in the inlet section becomes a much steeper drop in the ribbed section of the first leg. The second leg, which only extends to z=21.5, shows a similar trend with the rate of pressure loss being steeper in the ribbed section. Between each rib the pressure is seen to rise, which is followed by a large pressure drop across the rib. The pressure drop across the rib is associated with form drag. The drop is seen to be on the order of one half to one dynamic head. This is comparable to the experimental data shown in Rau et al. (1996).

Figure 8b shows $C_{p,rel}$ for the rotating case rot36. For this case the plot includes lines for y=0 and y=1 for each leg. The characteristics of each curve are similar to the stationary case. It is interesting to note that there is a difference of approximately one dynamic head between the leading and trailing surfaces. This pressure difference is the result of the combination of Coriolis and centrifugal forces, and is essentially an inviscid phenomenon. It is precisely this pressure difference which produces the secondary flows in a viscous flow. The pressure gradient is maintained across the axial extent of the channel even though the velocity must go to zero near the side walls. The lower velocity fluid near the walls does not have the centrifugal force to overcome the pressure gradient and thus succumbs to the pressure forces. Then, as a result of continuity, the flow located midway in the channel axially must flow against the pressure gradient. Another thing to notice about Fig. 8b is that the pressure jump, the form drag, across the ribs on the trailing surface of the first leg is greater than that on the leading surface. This effect is explained by the above argument because additional flow is supplied to the trailing surface. In the second leg, it is the leading surface which experiences larger pressure jump across the ribs since the flow is now radially inward.

Figure 9 shows the flow at several z locations for the case rot36 demonstrating the secondary flow which forms in each of the channel legs. Notice that in the outward flowing leg, leg 1, the core flow propagates toward the trailing surface forming a double vortex. For the inward flowing leg, at z=22 the opposite effect is visible. For larger values of z, near the turn, the second leg is dominated by a single strong vortex. One will notice that in later figures, which show mass transfer distributions, high levels of mass transfer are associated with regions of impingement in Fig. 9.

Heat/Mass transfer. The mass transfer is presented in the form of the Sherwood number normalized by the empirical

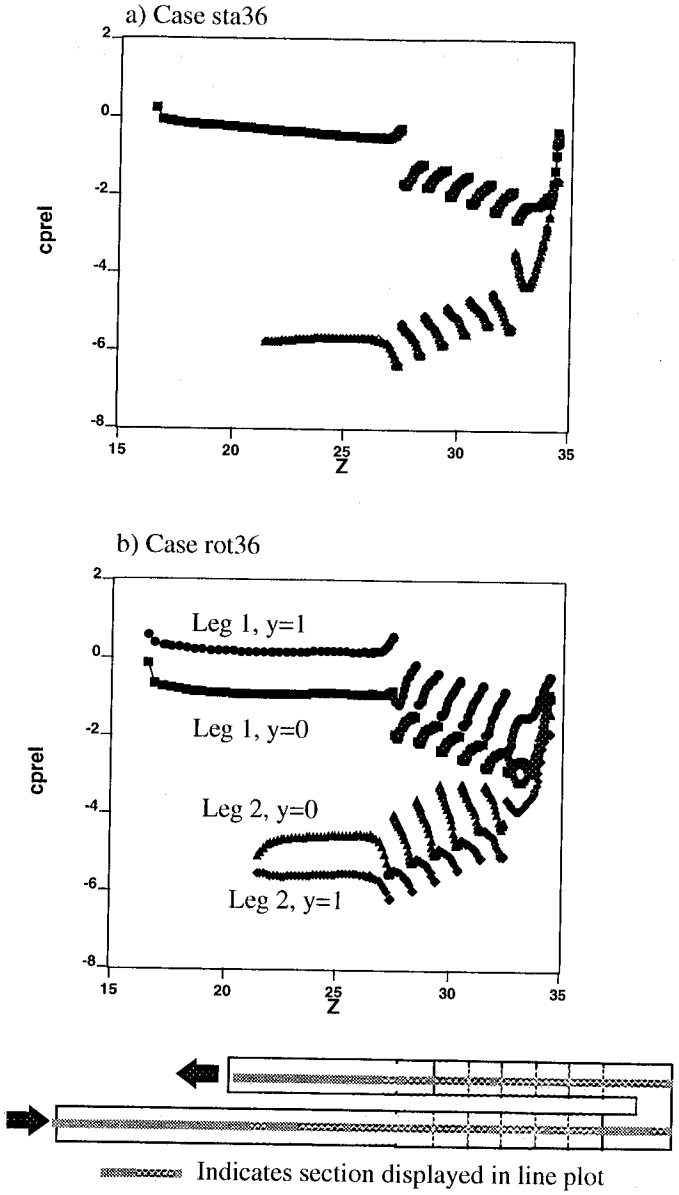

Fig. 8. Pressure on the centerline of the ribbed, a) case sta36, b) case rot36.

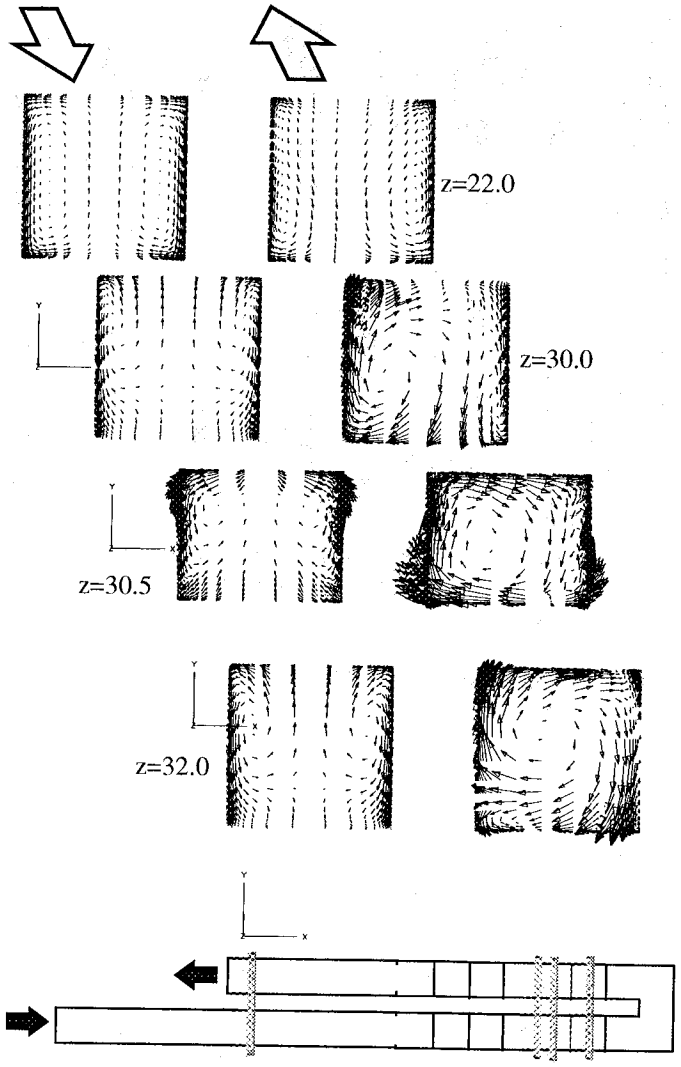

Fig. 9. Velocity vectors in several z planes for the case rot36. Cross sections on the left are radially outward and the leading wall is on the bottom.

value for fully developed turbulent pipe flow. The Sherwood number is defined as

$$Sh = \frac{h_m D}{\Lambda} \tag{10}$$

where D is the hydraulic diameter and Λ is the diffusion coefficient for naphthalene vapor in air. For the present work the Schmidt number was taken to be 2.28 as recommended by Park (1996).

The mass transfer coefficient h_m is defined by:

$$h_m = \frac{\dot{m}''}{C_w - C_b(s)} \tag{11}$$

The bulk total concentration, $C_b(s)$, is assumed to vary piecewise linearly between the inlet and the exit values, as was done in the experiment. Values of the bulk concentration was calculated at the beginning and end of each leg and used in the piecewise linear formula. The Sherwood number for fully developed turbulent pipe flow is taken to be

$$Sh_0 = 0.023 Re_D^{0.8} Sc^{0.4} \tag{12}$$

The heat transfer is presented in the form of the Nusselt number normalized by the empirical value for fully developed turbulent pipe flow. The Nusselt number is defined as

$$Nu = \frac{hD}{k} \tag{13}$$

where D is the hydraulic diameter and k is the thermal conductivity evaluated at the reference temperature. The reference temperature for the present study is taken to be the average film temperature. It is defined as:

$$T_{ref} = 0.5\left(\frac{T_{b,exit} + T_{b,in}}{2} + T_w\right) \tag{14}$$

a) Case sta36

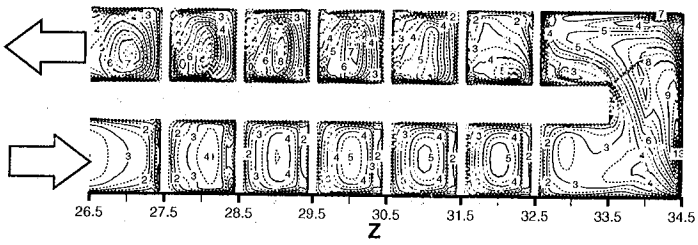

b) Case sta5

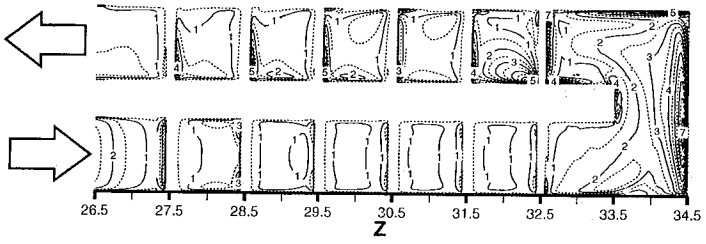

Fig. 10. Normalized Sherwood number, a) case sta36, b) case sta5.

The heat transfer coefficient h is defined by

$$h = \frac{q_w}{T_w - T_b(s)} \tag{15}$$

The bulk total temperature, $T_b(s)$, is assumed to vary piecewise linearly between the inlet and the exit values, similar to how the bulk concentration was handled. The Nusselt number for fully developed turbulent pipe flow is taken to be

$$Nu_0 = 0.023 Re_D^{0.8} Pr^{0.4} \tag{16}$$

Figure 10 shows the normalized Sherwood number on the ribbed surface for the stationary cases sta36 and sta5. From Fig. 10 it is immediately apparent that case sta5, with K_R=5 shows significantly less mass transfer than case sta36. Values near one between the ribs are a direct result of the lack of reattachment for the case sta5. Case sta36 on the other hand demonstrates levels and patterns which are characteristic of those presented in the literature. In the first leg peak values are located midway between ribs, roughly where reattachment occurs. In the turn, high values are seen near the endwall due the forcing of the flow downward from the impingement with the endwall. High values are again seen near the second outside corner for the same reason as it is seen near the endwall. Entering the second leg a peak is seen near the inside of the turn in the first rib pitch. Several rib pitches into the second leg the pattern begins to look periodic.

Figure 11 shows the mass transfer results for the rotating case rot36. The levels observed for this case are within the range observed in the experimental results. The patterns are also very similar to those of the experiment. Notice that, in general, the trailing surface in the first leg has higher values than the leading

a) Case rot36; Trailing Surface (y=1)

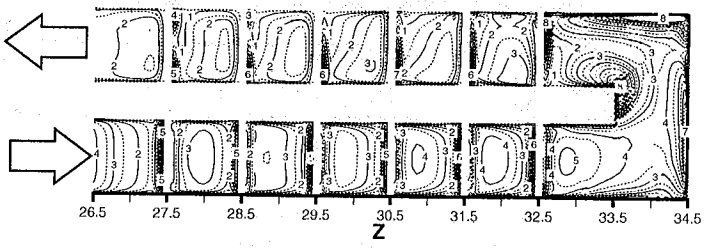

b) Case rot36; Leading Surface (y=0)

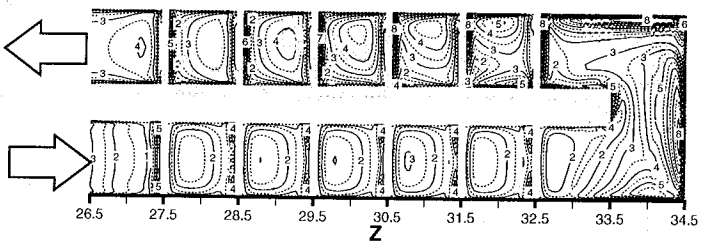

Fig. 11. Normalized Sherwood number for case rot36, a) Leading Surface (y=0), b) Trailing Surface (y=1).

surface. The opposite is true in the second leg. High values are seen on both surfaces near the endwall and near the outside of the second turn. Also seen in the experimental results of Park (1996) is the double peak in the first rib pitch in the second leg. Overall these results are quite encouraging. The overall pattern is strikingly similar to the experimental results.

Figure 12 shows the mass transfer results for the rotating case rot5, which had K_R=5. These results are characterized by

a) Trailing Surface (y=1)

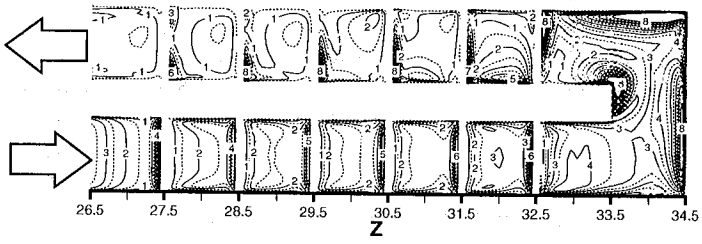

b) Leading Surface (y=0)

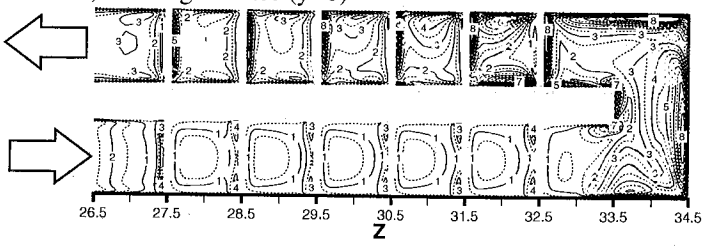

Fig. 12. Normalized Sherwood number for case rot5, a) Trailing Surface (y=1), b) Leading Surface

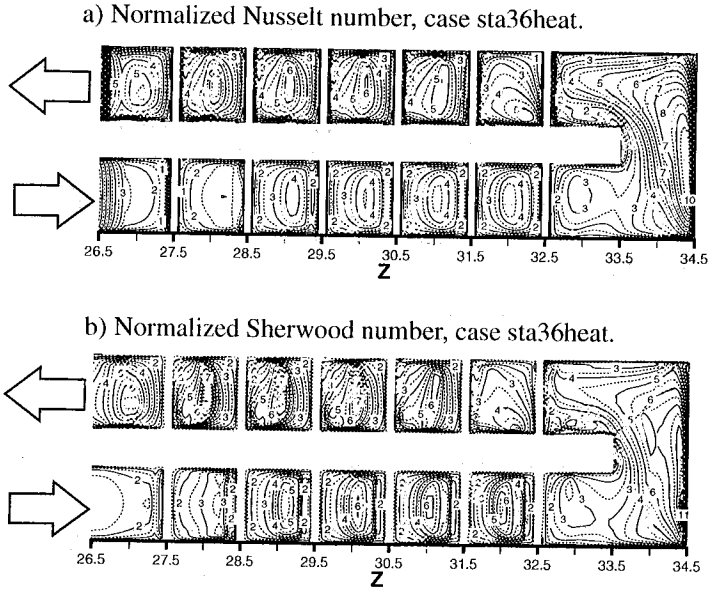

Fig. 13. Normalized Sherwood number and Nusselt number for the case sta36heat.

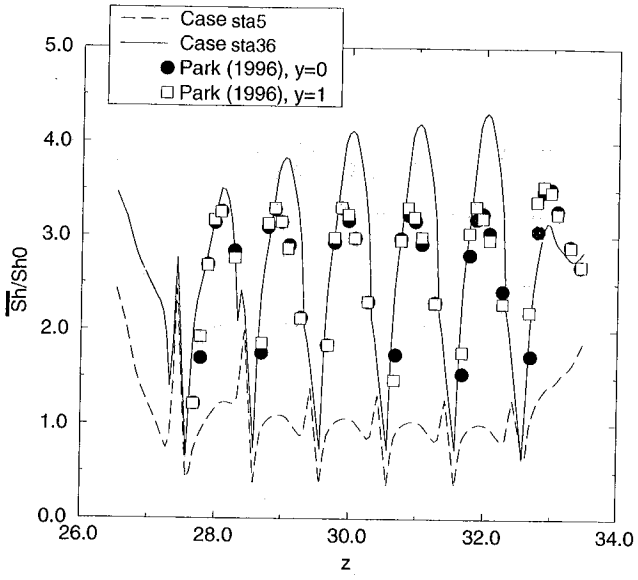

Fig. 14. Spanwise averaged Sherwood number for cases sta36 and sta5.

values which are too low in both legs. The results in the turn region are actually quite similar to the case rot36 which used K_R=36.

Figure 13 shows the mass transfer and heat transfer results for the cases sta36heat which is the case with an imposed wall temperature of $1.2T_{t,in}$. First comparing the mass transfer results to those shown in Fig. 10a, it can be seen that the patterns are very similar, however, the levels in the case sta36heat are somewhat higher than those in case sta36, the adiabatic case. Comparing the mass transfer and heat transfer results in Fig. 13 the patterns are seen to be similar as one would expect. The normalized heat transfer values are, in general, lower than the normalized mass transfer values. This may have to do with the variable properties introduced by the imposed temperature difference. However, another likely reason for a lower normalized heat transfer coefficient is the significant difference between the Prandtl number, 0.72, and the Schmidt number, 2.28. In Kayes and Crawford (1980) an empirical correlation attributed to Sleicher and Rouse (1975) is presented which is valid over a wide range of Prandtl number. If a Prandtl number of 2.28 is used in that correlation it produces a result roughly 15% higher than the correlation used to normalize the present results. This may imply that one should expect somewhat higher levels for the mass transfer values when normalized in the present manner.

Some quantitative comparisons with experimental results will now be made. Figure 14 shows the spanwise average mass transfer coefficient in the first leg for cases sta36, and sta5, along with the data of Park (1996). It is immediately apparent that the case sta5 predicts 70% too little mass transfer. The case sta36 compares quite well in the first pitch and then stays about 25% above the experimental results. Then at the end of the leg the numerical results once again agree with the data. Based on this figure it might be surmised that a value of K_R between 5 and 36 might match the data better. The present calculations are far too expensive to be testing a range of values for K_R, besides it seems much more likely that the results will be dominated by whether the flow attaches or not. While the case sta36 produces results which appear somewhat high compared to the data of Park (1996), when compared to a similar experiment by Chen et al. (1996) the agreement is better.

Figure 15 shows the normalized mass transfer coefficient down the centerline of the first leg of the channel for case sta36 along with the data of Chen et al. (1996). Only the fully developed portion of the calculation is placed on Fig. 15 for the sake of clarity. For this experiment the pitch to rib height ratio is 10.5, as compared to 10 for the present work. The data was digitized then normalized using a value of 2.5 for the Schmidt number, which is what is quoted in that paper. The data was then scaled down by 1.05 in the z-direction to match the present rib spacing. Comparison to this experiment, the case sta36 shows quite good agreement. In fact it agrees to within the experimental difference between the two walls which should have the same values.

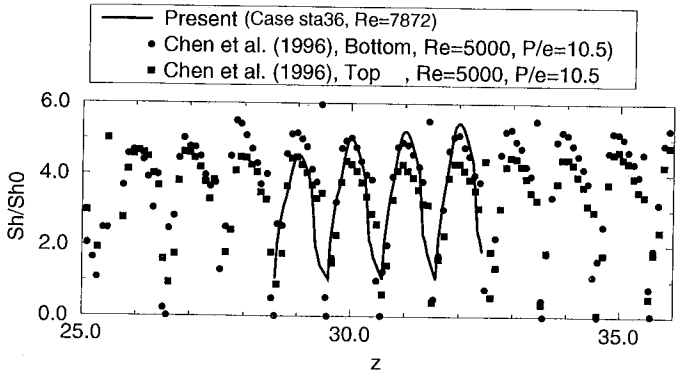

Fig. 15. Normalized Sherwood number down the centerline of the channel for the case sta36.

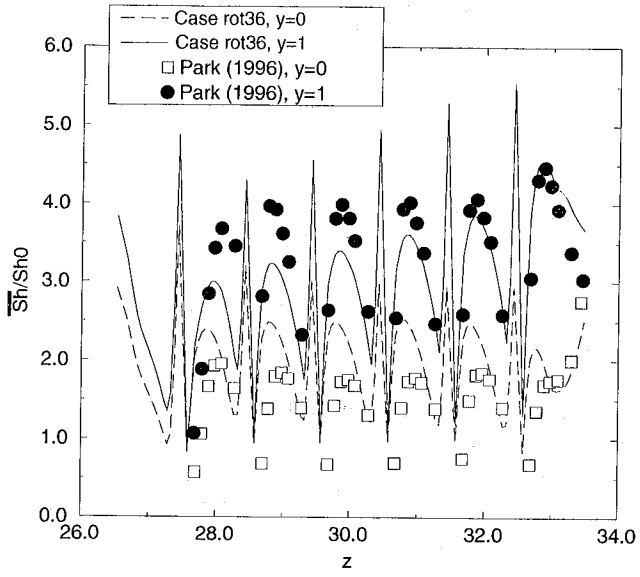

Fig. 16. Spanwise averaged Sherwood number in the first leg for the case rot36.

Figure 16 shows the spanwise averaged mass transfer coefficient in the first leg for the rotating case rot36 along with the data of Park (1996). For this case the trailing wall results agree well with the data, especially in the latter half of the leg. The leading wall values are somewhat higher than the data.

Figure 17 shows the results in the second leg for the case rot36. In the second leg the agreement with data is quite good for the trailing wall, especially in the downstream half. The leading wall on the other hand is generally under predicted.

Overall, the general trend for the rotating case seems to be to predict reasonably well the high mass transfer surface, while over and under predicting the low mass transfer surface in the first and second leg, respectively.

CONCLUSIONS

Calculations were presented for flow in a rotating ribbed channel with a 180 degree turn for Reynolds number in the range of 5250-7872, and Rotation number of 0.0 or 0.24. It was found that modifications were required to the ω wall boundary condition to predict the appropriate flow topology. Using the default value produced complete separation between the ribs, which is in contradiction to experimental observations. Once the ω boundary condition was modified such that the code correctly predicted flow attachment, agreement in many respects was improved. The flow structure observed experimentally was predicted with the present calculations. Also, by investigating the secondary flow patterns it is possible to associate regions of impingement with high heat/mass transfer regions. It was found that predicted heat/mass transfer patterns as well as averaged values agree well with experimental data.

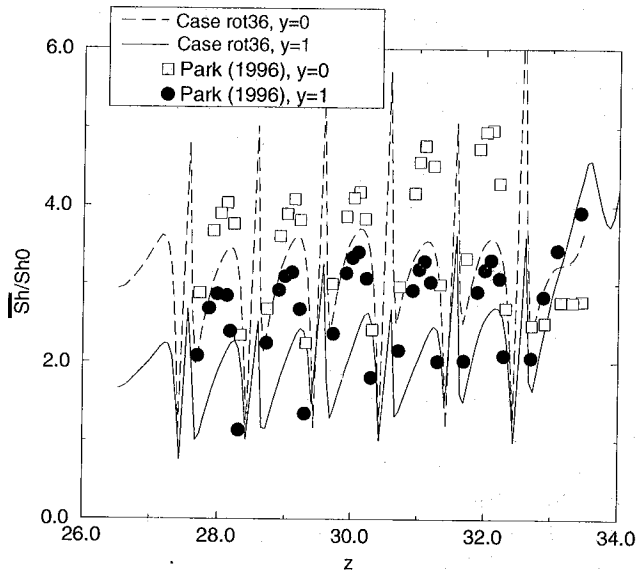

Fig. 17. Spanwise averaged Sherwood number in the second leg for the case rot36.

ACKNOWLEDGEMENTS

The present work was supported by the NASA Lewis Research Center as part of the Coolant Flow Management Program with funding from the Smart Green Engine Project. The author wishes to thank Mr. Steven Hippensteele, Dr. Raymond Gaugler, Chief of the Turbine Branch, Mr. Ned Hannum, Chief of the Turbomachinery and Propulsion Systems Division as well as to Dr. Louis Povinelli, Chief Scientist of the Turbomachinery and Propulsion Systems Division of NASA Lewis Research Center, for their support and encouragement of this work. In addition, the author would like to thank Dr. Ali Ameri, Dr. Erlendur Steinthorsson, and Mr. Robert Boyle for their many insightful conversations on these types of flows.

REFERENCES

Arnone, A., Liou, M.-S., and Povinelli, L. A.,1991, "Multigrid Calculation of Three-Dimensional Viscous Cascade Flows," AIAA-91-3238.

Arts, T., Lambert de Rouvroit, M., Rau, G. and Acton, P, 1992, "Aero-Thermal Investigation of the Flow Developing in a 180 Degree Turn Channel," VKI pre-print No 1992-10.

Besserman, D.L. and Tanrikut, S., 1991, "Comparison of Heat Transfer Measurements with Computations for Turbulent Flow Around a 180 Degree Bend", ASME paper 91-GT-2.

Boyle, R. J., "Heat Transfer in Serpentine Passages With Turbulence Promoters," 1984, NASA TM 83614.

Chen, Y., Nikitopoulos, D.E., Hibbs, R., Acharya, S. and Myrum, T.A., "Detailed Mass Transfer Distribution in a ribbed Coolant Passage," ASME paper 96-WA/HT-11.

Chima, R.V., 1996, "A k-ω Turbulence Model for Quasi-Three-Dimensional Turbomachinery Flows," To appear at AIAA Aerospace Sciences Meeting. Also NASA TM 107051.

Ekkad, S.V., Huang, Y. and Han, J.C., 1996a, "Detailed Heat Transfer Distributions in Two-Pass Smooth and Turbulated Square Channels with Bleed Holes," 1996 National Heat Transfer Conference, Houston, Texas, Vol. 8, pp. 133-140.

Ekkad, S.V., and Han, J.C., 1996b, "Detailed Heat Transfer Distributions in Two-Pass Square Channels with Rib Turbulators," Accepted to, 1996 International Journal of Heat and Mass Transfer.

"GRIDPRO,^{TM} /az3000, Users Guide and Reference Manual", 1993, Program Development Corporation, White Plains, NY.

"GRIDGEN, User's Manual for -," 1995, Pointwise, Inc.

Kays, W.M. and Crawford, M.E., 1980, "Convective Heat and Mass Transfer,", second Edition, MacGraw-Hill.

Hibbs, R.G., Acharya, S., Chen, Y., and Nikitopoulos, D.E., 1997, "Mass/Heat Transfer in a Ribbed Blade Coolant Passage with Cylindrical vortex Generators: The Effect of Generator-Rib Spacing," ASME paper 97-GT-161.

Liu, F. and Zheng, X., 1994, "A strongly-Coupled Time-Marching Method for Solving The Navier-Stokes and k-ω Turbulence Model Equations with Multigrid," AIAA-94-2389.

Menter, Florian R., 1992, "Improved Two-Equation k-ω Turbulence Models for Aerodynamic Flows," NASA-TM 103975.

Menter, Florian R., 1993, "Zonal Two Equation k-ω Turbulence Models for Aerodynamic Flows," AIAA-93-2906.

Park, C.W., "Local Heat/Mass Transfer Distributions in Rotating Two-Pass Square Channels," Ph.D. Dissertation, Department of Mechanical Engineering, Texas A&M University, College Station, TX, December, 1996.

Park, C.W., Lau S.C., and Kukreja, R.T., 1997, "Heat/Mass Transfer in a Rotating Two-Pass Square Channel with Transverse Ribs," Journal of Thermophysics and Heat Transfer, Vol. 11.

Prakash, P and Zerkle, R., 1992, "Prediction of Turbulent Flow and Heat Transfer in a Radially Rotating Square Duct," *Journal of Turbomachinery*, Vol. 114, pp.835-846.

Rau, G., Cakan, M., Moeller, D. and Arts, T., 1996, "The Effect of Periodic Ribs on the Local Aerodynamic and Heat Transfer Performance of a Straight Cooling Channel," ASME paper 96-GT-541.

Rigby, D.L., Ameri, A.A., and Steinthorsson, E., 1996a, "Internal Passage Heat Transfer Prediction Using Multiblock Grids and a k-w Turbulence Model," ASME paper 96-GT-188.

Rigby, D.L., 1996b, "Method of Weakest Descent for Automatic Block Merging," 15th Int. Conf. on Num. Methods Fluid Dynamics, Monterey, CA.

Rigby, D.L., Steinthorsson, E., and Coirier, W.J., 1997, "Automatic Block Merging Using the Method of Weakest Descent," AIAA paper no. 97-0197.

Schlichting, H., 1980, "Boundary-Layer Theory," Seventh Edition, McGraw-Hill Book Company.

Shen, J.R., Wang, Z., Ireland, P.T., Jones, T.V., Byerley, A.R., 1994, "Heat Transfer Enhancement Within a Turbine Blade Cooling Passage Using Ribs and Combinations of Ribs with Film Cooling Holes," *Journal of Turbomachinery*, Vol.118, pp. 428-434.

Sigal, A. and Danberg, J.E., 1990, "New Correlation of Roughness Density Effect on the Turbulent Boundary Layer," AIAA Journal Vol. 28, No. 3, pp 554-556.

Sleicher, C.A., and Rouse, M.W., Int. J. Heat Mass Transfer, vol. 18, 1975, pp. 677-683.

Snyder and Roelke, R.J., 1990, "Design of an Air-Cooled Metallic High Temperature Radial Turbine," *Journal of Propulsion and Power*, Vol. 6, pp. 283-288.

Steinthorsson, E., Liou, M.-S. and Povinelli, L.A., 1993, "Development of an Explicit Multiblock/Multigrid Flow Solver for Viscous Flows in Complex Geometries," AIAA-93-2380.

Stephens, M.A., Shih T. I-P., Civinskas, K.C., 1995a, "Effects of Inclined Rounded Ribs on Flow and Heat Transfer in a Square Duct," AIAA paper no. 95-2115.

Stephens, M.A., Shih, T. I-P., Civinskas, K.C., 1995b, "Computation of Flow and Heat Transfer in a Rectangular Channel with Ribs," AIAA paper no. 95-0180.

Stephens, M.A., Chyu, M.K., Shih, T. I-P., Civinskas, K.C., 1996, "Calculation and Measurements of Heat Transfer in a Square Duct with Inclined Ribs," AIAA paper no. 96-3163.

Stephens, M.A., Shih, T.I-P., 1997, "Computation of Compressible Flow and Heat Transfer in a Rotating Duct with Inclined Ribs and a 180-Degree Bend," ASME paper 97-GT-192.

Suo, M., 1978, "Turbine Cooling in the Aerothermodynamics of Aircraft Gas Turbines," AFAPL TR 78-52.

Taslim, M.E., Li, T., Spring, S.D., 1995, "Experimental Study of the Effects of Bleed Holes on Heat Transfer and Pressure Drop in Trapezoidal Passages With Tapered Turbulators," *Journal of Turbomachinery*, Vol.117, pp. 281-289.

Taylor, J.R., 1980, "Heat Transfer Phenomena in Gas Turbines," ASME 80-GT-172.

Tekriwal, P., "Heat Transfer Predictions in Rotating Radial Smooth Channel: Comparative Study of k-ε Models with Wall Function and Low-Re Model," ASME paper 94-GT-196.

Wagner, J.H., Johnson, B.V., Graziani, R.A., Yeh, F.C., "Heat Transfer in Rotating Serpentine Passages with Trips Normal to the Flow," *Journal of Turbomachinery*, Vol. 114, pp.847-857.

Wilcox, D.C., 1988,"Reassessment of the Scale-Determining Equation for Advanced Turbulence Models," AIAA Journal, Vol. 26, No.11, pp 1299-1310.

Wilcox, D.C., 1994a,"Turbulence Modeling for CFD," DCW Industries, Inc., La Canada, CA.

Wilcox, D.C., 1994b,"Simulation of Transition with a Two-Equation Turbulence Model," AIAA Journal, Vol. 32, No.2, pp. 247-255.

REPORT DOCUMENTATION PAGE

Form Approved
OMB No. 0704-0188

1. AGENCY USE ONLY (*Leave blank*)	2. REPORT DATE	3. REPORT TYPE AND DATES COVERED
	January 1999	Technical Memorandum

4. TITLE AND SUBTITLE

Prediction of Heat and Mass Transfer in a Rotating Ribbed Coolant Passage With a 180 Degree Turn

5. FUNDING NUMBERS

WU–523–26–13–00

6. AUTHOR(S)

David L. Rigby

7. PERFORMING ORGANIZATION NAME(S) AND ADDRESS(ES)

National Aeronautics and Space Administration
Lewis Research Center
Cleveland, Ohio 44135–3191

8. PERFORMING ORGANIZATION REPORT NUMBER

E–11300

9. SPONSORING/MONITORING AGENCY NAME(S) AND ADDRESS(ES)

National Aeronautics and Space Administration
Washington, DC 20546–0001

10. SPONSORING/MONITORING AGENCY REPORT NUMBER

NASA TM—1999-208501

11. SUPPLEMENTARY NOTES

Prepared for the 43rd Gas Turbine and Aeroengine Congress sponsored by the International Gas Turbine Institute of the American Society of Mechanical Engineers, Stockholm, Sweden, June 2–5, 1998. Responsible person, David L. Rigby, organization code 5820, (216) 977–1099.

12a. DISTRIBUTION/AVAILABILITY STATEMENT

Unclassified - Unlimited
Subject Categories: 07 and 34 Distribution: Nonstandard

This publication is available from the NASA Center for AeroSpace Information, (301) 621–0390.

12b. DISTRIBUTION CODE

13. ABSTRACT (*Maximum 200 words*)

Numerical results are presented for flow in a rotating internal passage with a 180 degree turn and ribbed walls. Reynolds numbers ranging from 5200 to 7900, and Rotation numbers of 0.0 and 0.24 were considered. The straight sections of the channel have a square cross section, with square ribs spaced one hydraulic diameter (D) apart on two opposite sides. The ribs have a height of 0.1D and are not staggered from one side to the other. The full three dimensional Reynolds Averaged Navier-Stokes equations are solved combined with the Wilcox k-ω turbulence model. By solving an additional equation for mass transfer, it is possible to isolate the effect of buoyancy in the presence of rotation. That is, heat transfer induced buoyancy effects can be eliminated as in naphthalene sublimation experiments. Heat transfer, mass transfer and flow field results are presented with favorable agreement with available experimental data. It is shown that numerically predicting the reattachment between ribs is essential to achieving an accurate prediction of heat/mass transfer. For the low Reynolds numbers considered, the standard turbulence model did not produce reattachment between ribs. By modifying the wall boundary condition on ω, the turbulent specific dissipation rate, much better agreement with the flow structure and heat/mass transfer was achieved. It is beyond the scope of the present work to make a general recommendation on the ω wall boundary condition. However, the present results suggest that the ω boundary condition should take into account the proximity to abrupt changes in geometry.

14. SUBJECT TERMS	15. NUMBER OF PAGES
Turbine cooling	18
	16. PRICE CODE: A03

17. SECURITY CLASSIFICATION OF REPORT	18. SECURITY CLASSIFICATION OF THIS PAGE	19. SECURITY CLASSIFICATION OF ABSTRACT	20. LIMITATION OF ABSTRACT
Unclassified	Unclassified	Unclassified	

NSN 7540-01-280-5500

Standard Form 298 (Rev. 2-89)
Prescribed by ANSI Std. Z39-18
298-102